Journal of The Electrochemical Society

Electrochemical Study of Butyl-Pyrene Nitrobenzoate Derivatives Trapped on MWCNT Nanostructured Electrodes

To cite this article: C. Barrientos *et al* 2021 *J. Electrochem. Soc.* **168** 126515

Journal of The Electrochemical Society, 2021 **168** 126515

Electrochemical Study of Butyl-Pyrene Nitrobenzoate Derivatives Trapped on MWCNT Nanostructured Electrodes

C. Barrientos,[1] R. Moscoso,[2] S. Moris,[3] and J. A. Squella[2,*,z]

[1]*Instituto de Ciencias Químicas Aplicada, Facultad de ingeniería, Universidad Autónoma de Chile, Chile*
[2]*Centro de Investigación de los Procesos Redox (CiPRex), Chemical and Pharmaceutical Sciences Faculty, University of Chile, 838492 Santiago, Chile*
[3]*Centro de investigación de estudios avanzados del Maule (CIEAM), Vicerrectoría de Investigación y Postgrado, Universidad Católica del Maule, Avenida San Miguel 3605, Talca 3480112, Chile*

In the scope of our studies tending to find new nanostructured electrodic platforms containing nitroaromatic compounds (NACs) capable of generating in situ electrocatalytic redox couples, we synthesized and electrochemically studied three related 4-(pyren-1-yl)-butyl-substituted nitrobenzoates (2-NBPy, 3-NBPy and 4-NBPy). The design of the compounds is based on a combination of a) an adsorptive tail (-butyl-pyrene) capable of interacting via π–π stacking with the MWCNT nanostructured electrodes and b) nitroaromatic compounds (NACs) capable of electrochemically activating to form a RNHOH/NO redox couple trapped on the nanostructured electrodic platform. Morphological and structural analyses of the nanostructured interfaces were performed by SEM and WAXS/SAXS analysis. All of the NBPy compounds trapped on the nanostructured electrodic platform were susceptible to reduction, generating the corresponding hydroxylamine derivative. The order of ease of reduction for the nitrocompounds is 4-NBPy > 2-NBPy > 3-NBPy. After electrochemical activation, all compounds generated an RNHOH/NO redox mediator couple with the following order of stability of the mediator couple: 2-NBPy > 3-NBPy > 4-NBPy. For the 2-NBPy and 3-NBPy derivatives, excellent stability of the couple was observed, and a decrease in the peak current of 6% was observed after 60 min.
 [DOI: 10.1149/1945-7111/ac3ff5]

Manuscript submitted August 31, 2021; revised manuscript received November 30, 2021. Published December 14, 2021. *This paper is part of the JES Focus Issue on Modern Electroanalytical Research in the Society for Electroanalytical Chemistry (SEAC).*

The evolution of the electrode phases has occurred by incorporating new materials that have evolved from purely conductive electrodic phases (donating or accepting electrons from species in solution) to phases that, in addition to fulfilling the basic role of electronic exchange, provide other characteristics, such as adsorption, catalysis, and chemical affinity. In this scope, carbon-based materials such as carbon nanotubes (CNTs) have modified the concept of the classic electrode/solution interface by changing the approach to electrochemistry.[1–6] CNTs are carbon allotropes consisting of C sp^2 hybridizations, such as rolled graphene sheets, and exist in two main forms: a) single walled carbon nanotubes (SWCNTs), which consist of a single tube of rolled graphene with lengths of 0.2–5 μm and diameters of 1–2 nm, and b) multiwalled carbon nanotubes (MWCNTs), which consist of various concentric tubes of rolled graphene. CNTs have attracted increasing attention since their discovery due to their good electrical conductivity, nanometer size, lack of toxicity, high surface area, significant mechanical strength, good chemical stability, functionalization possibility and excellent adsorption properties.[7–12] Tailoring the electrochemical interface with redox molecular assemblies is a fascinating approach used to develop versatile platforms for catalytic and sensing applications. In these cases, surface-adsorbed redox molecules have important roles in controlling the electron transfer reactions at the interface. Various research groups have attempted to design these interfaces; however, the search for new molecules with strategic functional groups continues and has been a way to connect organic chemistry and electrochemistry.[13]

There are several ways to modify CNT interfaces and provide support for the development of nanostructured electrode platforms. A covalent modification involves the formation of covalent bonds in the CNT wall, which changes the sp^2 hybridization of the carbon atoms to sp^3; this change affects the conductive properties of CNTs due to a loss of π electrons in the structure.[14,15] The loss of conductivity causes a decrease in electrochemical activity, which is not advantageous for an electrode material. On the other hand, noncovalent functionalization relies on physical adsorption that is based on weak interactions (e.g., interactions). Noncovalent functionalization is particularly attractive because it offers the possibility of attaching chemical handles, thus preserving the sp^2 nanotube structure and consequently not affecting the electronic network.[16–18] In our laboratory, we utilized this last strategy, publishing several works modifying MWCNTs with nitroaromatic compounds (NACs).[19–24]

On the other hand, there is a very interesting paper wherein Giroud et al.[25] reported the functionalization of MWCNT electrodes by a bifunctional nitroaromatic molecule accomplished via π–π interactions of a pyrene derivative. DTNB (5,5′-dithiobis (2-nitrobenzoic acid)) possesses both electroactivable nitro groups and negatively charged carboxylic groups. Therefore, taking advantage of the π–π stacking of pyrene on CNT sidewalls, they reported the innovative noncovalent immobilization of DTNB on MWCNT coatings and investigated the electrochemical properties for NADH oxidation through the electrochemical activation of nitro substituents into hydroxylamine groups. We have tested a rather different strategy that is also based on the π–π stacking of pyrene. In our case, instead of fixing the pyrene derivative to the MWCNT layer, we modified the NAC with an "adsorptive tail" of butylpyrene, which in turn is trapped in MWCNTs by π–π stacking.[26–28] In that paper, we demonstrated the usefulness of a new idea, which is to attach an "adsorptive tail" to the nitroaromatic compound (NAC), substantially increasing the strength of the GCMWCNT-NAC interaction and increasing the stability of the electrode. In fact, the π–π stacking interactions of the pyrene adsorptive tail favor the stability of NAC on the nanostructured electrode platform.

With the aim of designing molecules with a high capacity to be retained on the electrode in this work, we synthesized three related 4-(pyren-1-yl)-butyl-substituted nitrobenzoate derivatives (2-NBPy, 3-NBPy and 4-NBPy), and we studied the effect of the molecular structure on the electrochemical behavior and the interaction with the nanostructured electrode platform.

Experimental

Reagents and materials.—All analytical grade reagents were purchased from Sigma-Aldrich and used without further purification. Britton Robinson buffer (0.1 M) was used as a working solution. Before each experiment, the working solutions were purged with

*Electrochemical Society Member.
[z]E-mail: asquella@ciq.uchile.cl

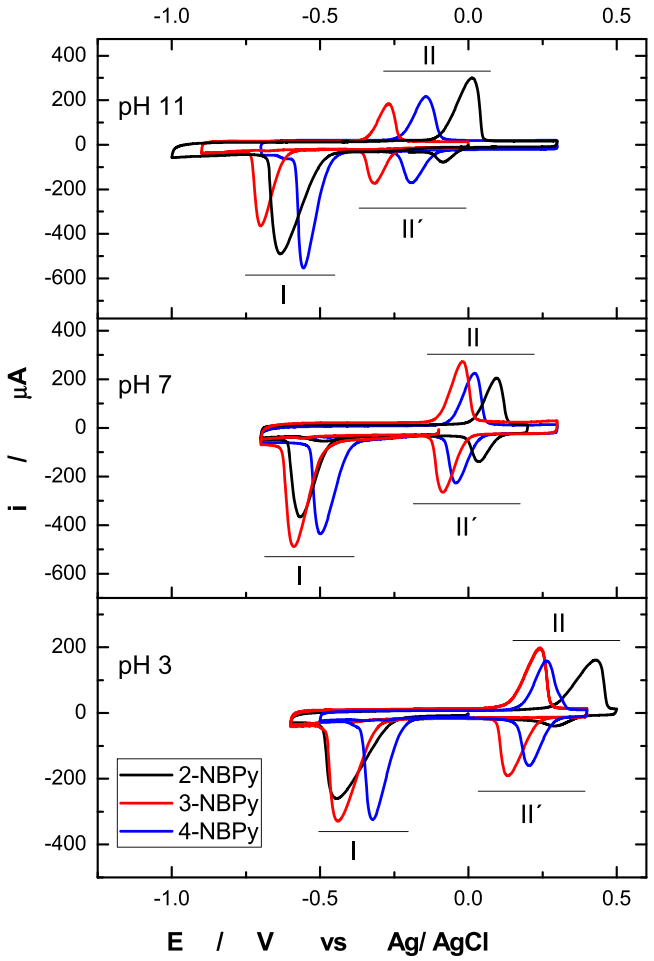

Figure 1. Cyclic voltammograms of 2-NBPy, 3-NBPy and 4-NBPy entrapped on GCMWCNTs in 0.1 M Britton-Robinson buffer at pH 3, 7 and 11 under a 100 mVs^{-1} sweep rate.

extra pure nitrogen. The pH of the solutions was adjusted by a WTW model pMx 3000 pH meter. Multiwalled carbon nanotubes (MWCNTs) 1.5 μm in length and 10 nm in diameter were purchased from Dropsens S.L., Spain.

The melting point of the synthesized compounds was determined using a Kofler camera Bock monoscope. A 300 MHz spectrometer (Bruker, WM 300) for 1H NMR and 13C NMR analysis was used.

General Procedures

Synthesis of 4-(pyren-1-yl)butyl nitrobenzoate derivatives.— Equimolar quantities of the respective nitrobenzoyl chloride and 4-pyren-1-ylbutanol were mixed in a round bottom flask with dry THF to obtain the 4-(pyren-1-yl)butyl nitrobenzoate derivatives, according to previously reported methodology.[26]

Crystal structure.—Crystals of 4-(pyren-1-yl) butyl-2-nitrobenzoate were prepared by dissolving the polycrystalline material in boiling chloroform (0.5 ml), and then hot methanol was added dropwise (0.5 ml). The mixture was allowed to crystallize for one week until the appearance of yellow plates. The X-ray data at 150 K were collected with a D8 VENTURE Bruker AXS diffractometer using Mo$K\alpha$ radiation ($\lambda = 0.71073$ Å). The structures were solved by using OLEX2 with olex2.refe using charge flipping and refined with the SHELXL refinement package. H atoms were finally included in their calculated positions and treated as riding on their parent atom with constrained thermal parameters, and the constraint distances of C—H ranged from 0.95 Å to 1.00 Å.

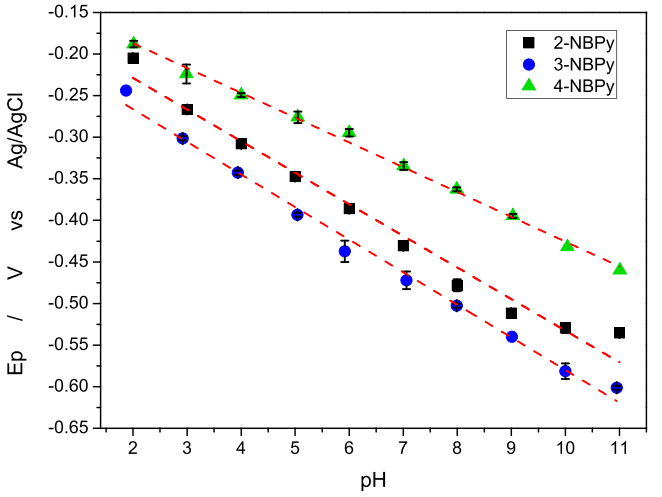

Figure 2. *Ep* vs pH plots from differential pulse voltammetry for nitro reduction of 2-NBPy, 3-NBPy and 4-NBPy entrapped on GCMWCNTs in 0.1 M Britton-Robinson buffer.

Synthesis of 4-(pyren-1-yl)butyl nitrobenzoate derivatives.—4-(pyren-1-yl) butyl-2-nitrobenzoate. (2-NBPy) $C_{27}H_{21}NO_4$. Yellow powder, yield: 53.52%, mp:135 °C–136 °C, ^{1}*H-NMR (DMSO-d_6 δ (ppm)):* 8.41–7.95, (m, 10H, Ar-H), 7.86–7.76, (m, 3H, Ar-H), 4.36, (t, 2H, CH_2 -OR), 3.38, (c, 2H, CH_2-pyrene), 1.96–1.79, (m, 4H, 2xCH_2). ^{13}*C-NMR (*75 MHz*, DMSO-d_6 δ (ppm)):* 165.18, 148.43, 137.09, 134.06, 133.32, 131.36, 130.88, 130.33, 129.75, 128.55, 127.94, 127.67, 126.97, 126.82, 126.61, 125.41, 125.25, 124.69, 124.62, 124.56, 123.96, 66.39, 32.60, 31.17, 28.27.

4-(pyren-1-yl)butyl-3-nitrobenzoate (3-NBPy) $C_{27}H_{21}NO_4$. Yellow powder, yield: 52.24%, mp: 107 °C–108 °C, ^{1}H-NMR (DMSO-d_6 δ (ppm)): 8.63–7.95, (m, 12 H, Ar-H), 7.77, (q, 1 H, Ar-H), 4.43, (t, 2 H, CH_2-OR), 3.44, (c, 2 H, CH_2-pyrene), 2.1–1.8, (m, 4 H, 2xCH_2). ^{13}*C-NMR (75 MHz, CDCl$_3$ δ (ppm)):* 164.44, 148.29, 137.06, 135.55, 131.70, 131.34, 131.10, 130.85, 129.75, 128.54, 128.12, 127.98, 127.91, 127.67, 126.96, 126.60, 125.40, 125.24, 124.70, 124.59, 123.90, 65.83, 32.60, 31.17, 28.44.

4-(pyren-1-yl)butyl-4-nitrobenzoate (4-NBPy) $C_{27}H_{21}NO_4$. Yellow powder, yield: 58.64%, mp: 168 °C-169 °C, ^{1}*H-NMR (CDCl$_3$) δ (ppm)*: 8.22–7.76 (m, 12H, Ar-H), 4.34, (t, 2 H, CH_2 -OR), 3.36, (t, 2 H, CH2-pyrene), 2.05–1.80 (m, 4H, 2xCH_2). ^{13}*C-NMR (75 MHz, CDCl$_3$ δ (ppm)):* 163.62, 149.34, 134.96, 134.54, 130.39, 129.80, 129.48, 128.92, 127.57, 126.46, 126.31, 125.71, 124.91, 124.00, 123.76, 122.37, 122.15, 94.06, 64.67, 63.55, 32.00, 28.68, 27.38, 26.88.

Scanning electron microscopy (SEM).—The morphology was investigated by SEM using an Inspect Scanning Electron Microscope F-50 operated at 10 kV All SEM measurements were carried out on glassy carbon discs (TED Pella Brand, Inc. (N16524)) measuring 12.7 mm in diameter modified with MWCNTs or MWCNTs and NBPy.

Wide (WAXS) and small (SAXS) angle X-ray scattering.—All samples for WAXS/SAXS analysis were prepared by filtering a 10 ml carbon nanotube dispersion. Whatman nylon membrane filters were used (pore size of 0.45 μm). The filter paper with the nanotubes was allowed to dry and then cut into 1 cm diameter discs for WAXS/SAXS analysis. Modification with NAC was carried out by directly adding 5 microliters of nitro compound solution and allowing it to dry.

WAXS was carried out in an Anton Paar SAXSpoint2.0 SAXS/WAXS/GISAXS system, with an Eiger R 1 M detector and a Primus100 microfocus copper source at 50 kV and 100 μA monochromated by an ASTIX multilayer mirror (wavelength

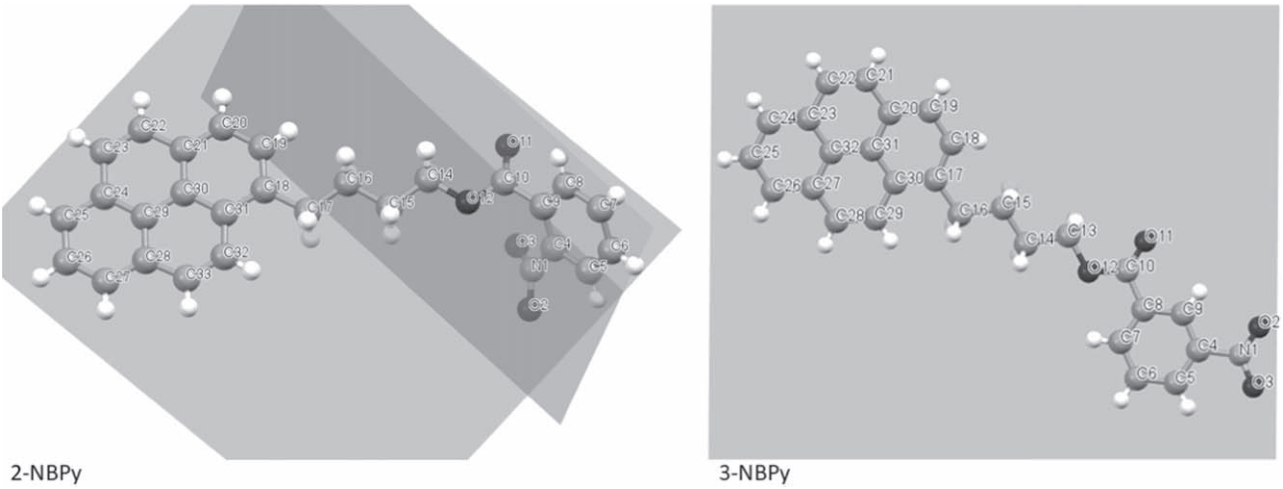

Figure 3. 3D molecular structures of 2- and 3-NBPy derivatives.

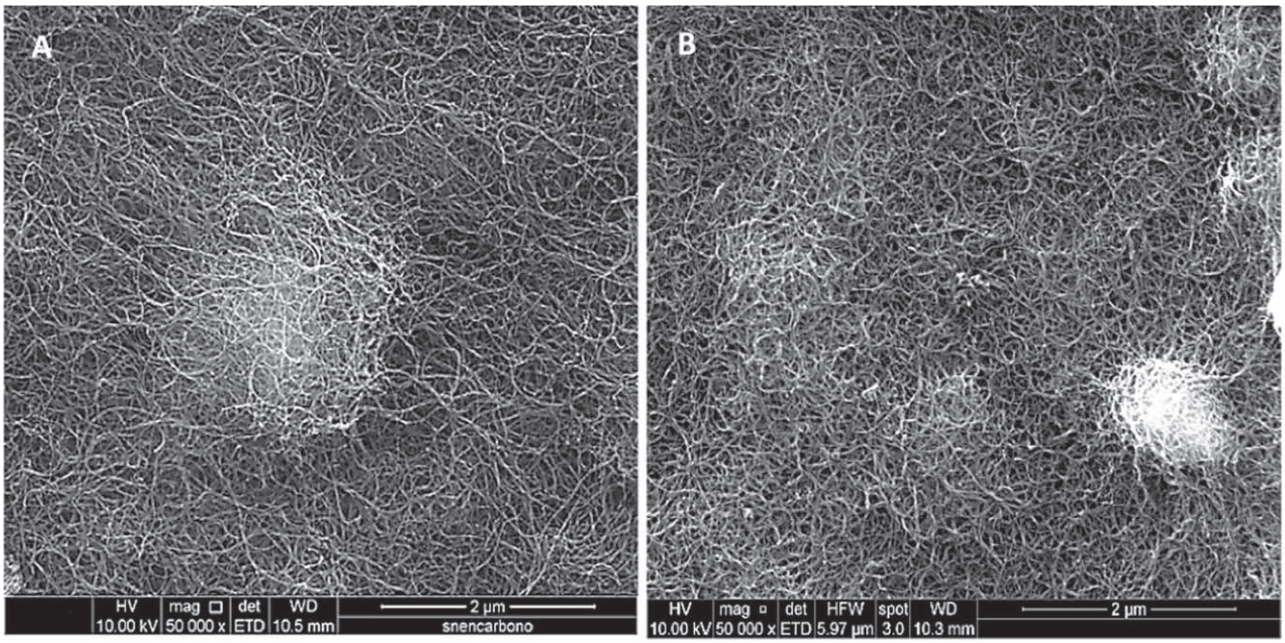

Figure 4. SEM image obtained for (A). a GC-MWCNT nanostructured platform and (B). a GCMWCNT nanostructured platform modified with 2-NBPy and 0.5 mM Britton-Robinson buffer at pH 7. Magnification of 50,000X; scale bar of 2 μm.

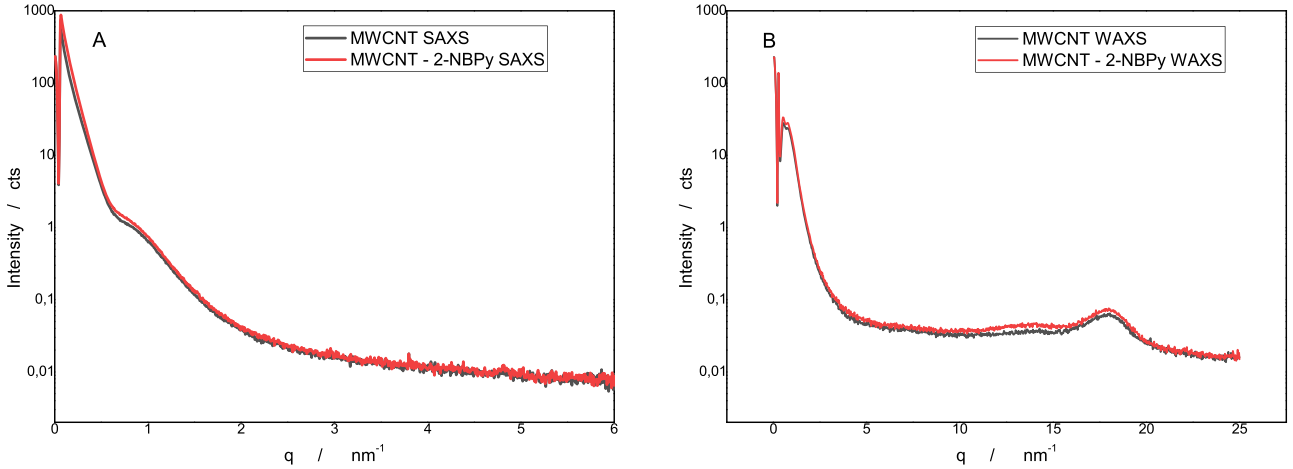

Figure 5. SAXS (A) and WAXS (B) patterns of the MWCNT nanostructured platform with and without 2-NBPy.

CuKalpha1–2 = 1.5418 Å), yielding point collimation. The sample was directly mounted as a single layer on a transmission sample holder and measured statically in vacuum (no rotation and not confined in mylar or Kapton films). WAXS was measured at a sample detector distance of 11.68 mm, and SAXS was measured at 56.35 mm, averaging 24 frames of 300 s exposition time each. The sample was measured at room temperature (302.5 K).

Electrochemical measurements.—Electrochemical measurements in a conventional three-electrode cell previously degassed by bubbling N_2 for 10 min were performed. Voltammetric curves on a CHI-650 (CH Instruments Inc., USA) equipment were recorded. A 3-mm-diameter glass carbon electrode (GCE) (Model CHI104, CH Instruments) was used as the working electrode. A platinum wire (BASiMW-1032) and Ag/AgCl/NaCl (0.3 M) (BASi MF-2052) were used as auxiliary and reference electrodes, respectively.

Preparation of MWCNT dispersion.—A 3 mg ml^{-1} MWCNT dispersion in 1,3-dioxolane was prepared and sonicated three times for 5 min each. The refrigerated dispersion was stored for further use.

Preparation of modified electrodes.—Glassy carbon electrodes with 0.3 and 0.05 μm aluminum oxide were polished. Then, 5 μl of MWCNT dispersion was dropped on the surface of the electrode and dried at ambient temperature, and GCMWCNTs were obtained. Subsequently, the GCMWCNTs were modified by immersion for 10 s in 0.5 mM nitro aromatic compounds (NBPy), obtaining the modified electrode GCMWCNT-NBPy, which was washed with water and then immersed in a cell containing only Britton-Robinson buffer for voltammetry experiments.

Voltammetric measurements.—The nitro-functionalized GCMWCNT-NBPy electrodes were immersed in an electrochemical cell containing only the supporting electrolyte (without NBPy derivatives in solution) and submitted to the corresponding potential scan. All experiments were carried out at room temperature (25 ± 1 °C).

Results

Electrochemical behavior of entrapped NBPy compounds on GCMWCNTs.—We have previously demonstrated how the π-π stacking interactions of the pyrene adsorptive tail improve the stability of nitro aromatic compounds on the nanostructured electrode platform and the electrocatalytic activity of some of these compounds in the oxidation of NADH.[26] In this study, we investigate how structural changes in the trapped molecule can affect the electrochemical behavior.

The modified GCMWCNT-NBPy electrode was immersed in a cell containing only 0.1 M Britton-Robinson buffer at pH 3, 7 and 11, respectively. By application of a cathodic potential sweep starting at—0.1 V up to the reduction peak, the corresponding NBPy compound was transformed in situ into the corresponding hydroxylamine derivative, generating peak I (Fig. 1), according to Eq. 1:

$$R\,NO_2 + 4H^+ + 4e^- \rightarrow RNHOH + H_2O \quad [1]$$

Subsequently, after the first reduction peak, the sweep direction was reverted in an anodic sweep until the total appearance of an oxidation peak. In this sweep, the corresponding hydroxylamine derivative is oxidized to a nitroso derivative, generating peak II, according to Eq. 2:

$$RNHOH \rightarrow RNO + 2H^+ + 2e \quad [2]$$

Following a second consecutive cathodic scan and starting at + 0.3 V up to −0.7 V, it was possible to see the appearance of peak II', which corresponds to the reduction of the corresponding nitroso derivative to the corresponding hydroxylamine derivative according to Eq. 3:

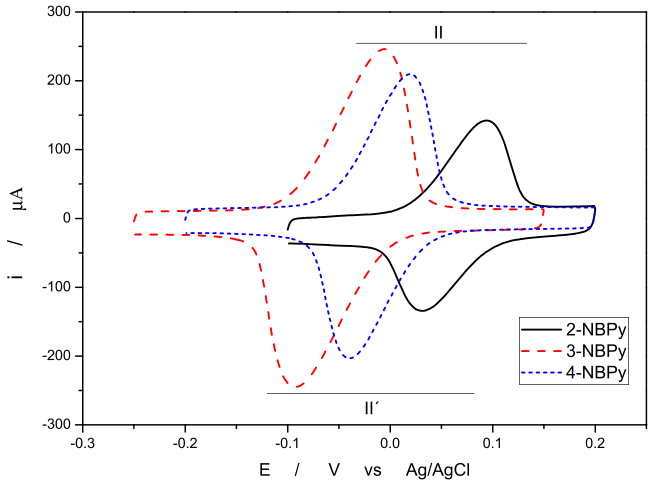

Figure 6. Cyclic voltammogram of the isolated RNHOH/RNO redox pair of 2−, 3− and 4−NBPy entrapped on GCMWCNTs in 0.1 M Britton-Robinson buffer at pH 7 at 100 mVs^{-1}.

$$RNO + 2H^+ + 2e \rightarrow RNHOH \quad [3]$$

Furthermore, according to the above Eq. 1, all of the NBPy derivatives follow a pH-dependent reduction, as verified by the behavior of Ep vs pH, as shown in Fig. 2. The potential pH dependence was studied using the VPD technique at different pH values for NBPy derivatives. All NBPy derivatives show pH dependence in the range between 2–11, and when the pH increased, the peak potential was shifted to a more negative value. The slope values were approximately −40 mV pH^{-1}, and other nitro compounds showed a similar slope value for the irreversible reduction of the nitro group. The behavior described above for the NBPy compounds adsorbed on the nanostructured electrodic platform follows the same classical behavior very well described for nitro aromatic compounds (NACs) in solution.[29–31]

According to the voltammograms of Fig. 1 and Ep vs pH of Fig. 2, 4-NBPy is the easiest compound to reduce, as it has the least negative reduction potential of the series, which is mainly due to the conjugation of the nitro with the carbonyl of the ester group. In the case of the 2-NBPy compound, there is a loss of the conjugation of the nitro with the carbonyl ester because both groups are not coplanar, thus leaving only the inductive effect. The nitro group for 2-NBPy has a slightly less negative reduction potential than 3-NBPy, which is due exclusively to its proximity to the carbonyl ester group.

To demonstrate the nonplanar character of the 2-NBPy compound, single crystal XRD analysis was performed and compared with that previously reported for 3-NBPy.[32] The torsion angle between the aromatic ring and carbonyl group corresponds to −117.0° for O12—C10—C9—C8, the torsion angle between the nitro group and aromatic ring is −147.1° for O3—N1—C4—C5, and it is −151.6° for O2—N1—C4—C9 in 2-NBPy. In contrast to the 3-NBPy compound, both the nitro group and the aromatic ring belong to the main plane of the molecule. As seen in Fig. 3, the carbonyl ester group is not coplanar with the nitrophenyl group for 2-NBPy, unlike the 3-NBPy compound, where the carbonyl ester is coplanar with the nitrophenyl group. This structural difference affects its electronic properties.

Figures 4A and 4B show SEM images of the nanostructured electrode platforms modified with and without nitro compounds. No major difference is observed between the images. Figure 4B does not show the presence of clusters or aggregates other than the carbon nanotubes attributable to 2-NBPy. The nitro compound is

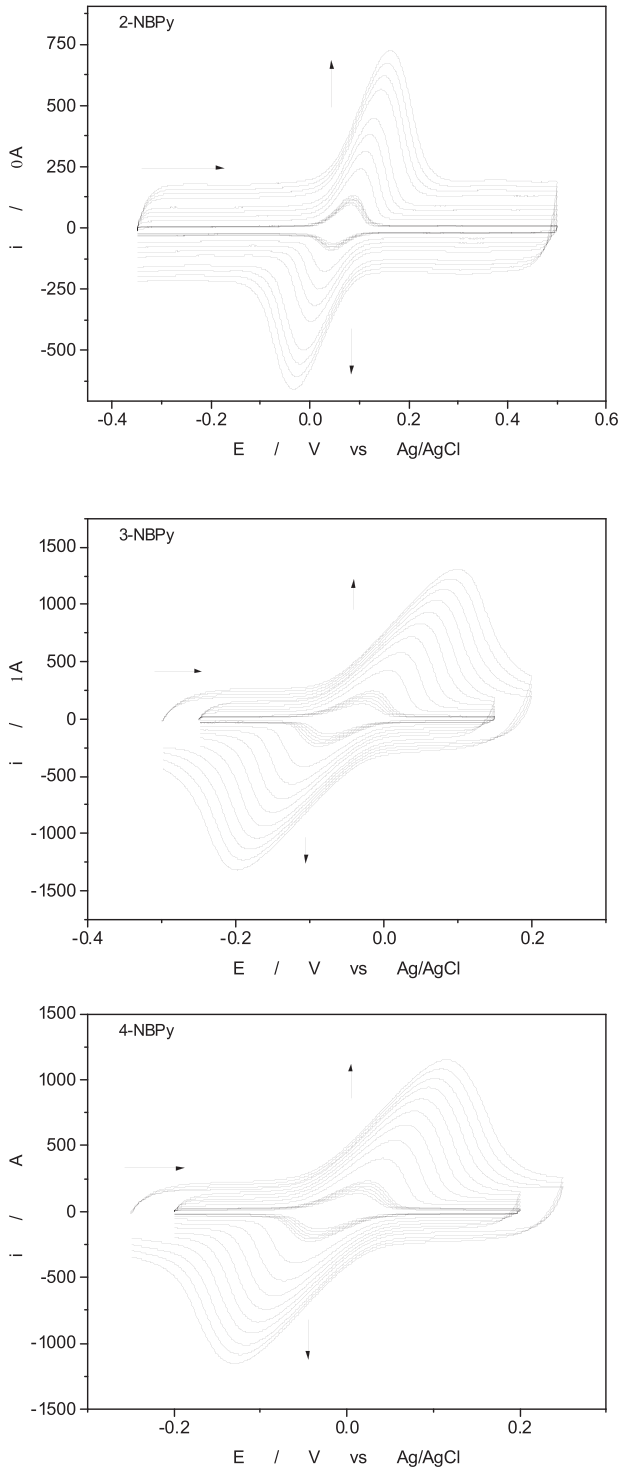

Figure 7. Cyclic voltammogram of the isolated RNHOH/RNO redox pair of 2−, 3−, and 4-NBPy entrapped on GCMWCNTs in 0.1 M Britton-Robinson buffer at pH 7 under a sweep rate of 0.1 Vs^{-1} to 1 Vs^{-1}.

completely distributed by the 3D nanostructure that forms the electrode, occupying the interstices between the nanotubes in a homogeneous way. The SEM image is not sensitive to the presence of the nitrocompound as the electrochemical technique is.

WAXS and SAXS can be very valuable tools to characterize the structure of MWCNTs.[33,34] We also apply these techniques to our nanostructured platforms. The SAXS and WAXS patterns of MWCNTs and MWCNT-2-NBPy are exhibited in Fig. 5. The SAXS diffraction intensity of MWCNTs is similar to that of MWCNT-2-NBPy (Fig. 5A), which could be caused by the homogeneous ordering of 2-NBPy in MWCNT-2-NBPy not affecting the intensity of the SAXS diffraction compared with that of the MWCNTs. On the other hand, the radial intensity profile, according to the WAXS results (Fig. 5B), reveals the presence of a peak corresponding to the approximately 18 nm^{-1} characteristics of the 002 reflection from the graphite layer structure of the MWCNTs. The above results allow us to affirm that the entrapped butylpyrene nitroaromatic derivative in the nanotube network is between the interstices and not inside the nanotubes.

Electrochemical behavior of entrapped hydroxylamine/nitroso derivatives (RNHOH/RNO) from NBPy.—One of the main characteristics of the electrochemistry of NAC adsorbed on a nanostructured electrodic platform is that the redox pair formed between the nitroso and hydroxylamine derivatives produces a persistent couple (peaks II/II'), which can act as a redox mediator in important reactions such as the oxidation of NADH.[35–39]

By suitably adjusting the parameters of the potential sweep, the couple corresponding to the II/II ' redox pair can be obtained and studied in isolation (Fig. 5). Furthermore, from the cyclic voltammograms of NBPy derivatives at different scan rates, namely, 0.05 $V\,s^{-1}$ to 1 $V\,s^{-1}$ (Fig. 6), it is possible to apply Laviron's method to calculate the heterogeneous electron transfer rate constant for the RNHOH/RNO couple entrapped in the multiwalled carbon nanotubes.[40] Ep_a and Ep_c vs Log v were plotted. A linear fit at high scan rates ($\Delta Ep = 0.2$ V/n, where n is 2 according to Eq. 2) was applied. From the slopes of the linear fit in Fig. 7, heterogeneous transfer coefficients, α, were obtained from Eqs. 3 and 4.

$$m_c = -\frac{2.303RT}{\alpha_c nF}(cathodic\ branch) \qquad [3a]$$

$$m_a = \frac{2.303RT}{(1-\alpha_a)nF}(anodic\ branch) \qquad [4]$$

where m_c and m_a are the experimental cathodic and anodic slopes, respectively. α_c and α_a are the cathodic and anodic transfer coefficients, respectively. In Table I the linear fitting parameters of Laviron´s plot are shown. Furthermore, Table II shows the experimental transfer coefficient for all compounds. With an α value close to 1, a product-like activated complex in the reaction is expected, and with an α value close to 0, a reactant-like activated complex is expected. For the reduction process, α_c values between 0.25–0.29 were observed. Thus, a reactant-like activated complex, R-NO, is expected for the reduction process, and a product-like activated complex, R-NO, is expected for the oxidation process, according to Eq. 2. Considering the α values, a similar pathway for the oxidation and reduction process is expected in the mechanism.

Table I. Linear fitting parameters of Laviron's plot.

Compound	Slope anodic branch	Slope cathodic branch	r^2
2-NBPy	0.119 ± 0.035	−0.110 ± 0.020	r^2_a: 0.971; r^2_c: 0.981
3-NBPy	0.124 ± 0.012	−0.117 ± 0.010	r^2_a: 0.982; r^2_c: 0.981
4-NBPy	0.104 ± 0.011	−0.102 ± 0.010	r^2_a: 0.995; r^2_c: 0.991

where r^2_a corresponds to the anodic linear fit and r^2_c corresponds to the cathodic linear fit.

Table II. Experimental heterogeneous transfer coefficients for NBPy derivatives.

Compound	α_a	α_c
2-NBPy	0.751	0.269
3-NBPy	0.761	0.253
4-NBPy	0.716	0.290
3,5-DNBPy[26]	0.79	0.22

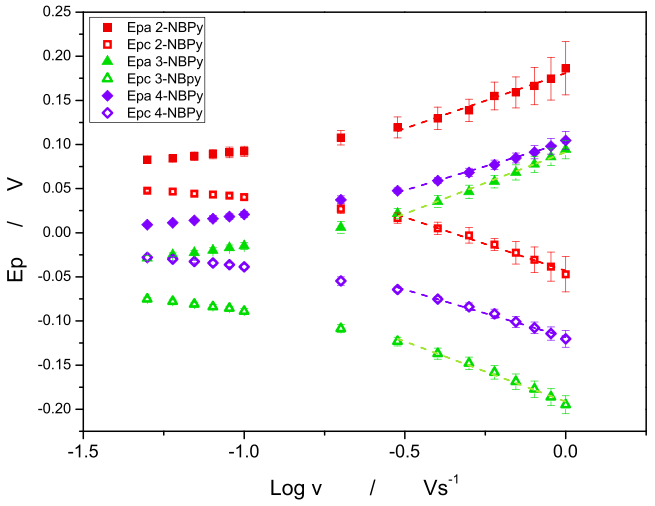

Figure 8. Laviron´s plot of 2−, 3−, and 4-NBPy compounds.

Table III. Heterogeneous electron transfer rate constant for NBPy derivatives.

Compound	*ks* cat (s^{-1})	*ks* anod (s^{-1})	*ks* mean (s^{-1})
2-NBPy	2.4	2.2	2.3
3-NBPy	1.4	1.4	1.4
4-NBPy	2.0	1.9	2.0
3,5-DNBPy[26]	—	—	1.7

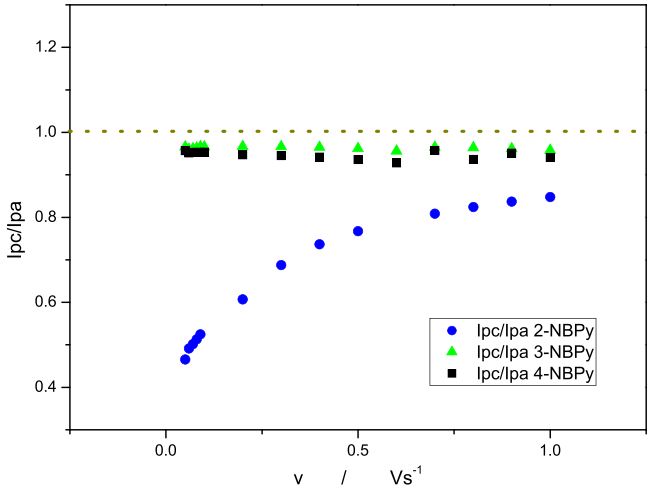

Figure 9. Current ratio plot vs sweep rate of 2−, 3−, and 4-NBPy compounds.

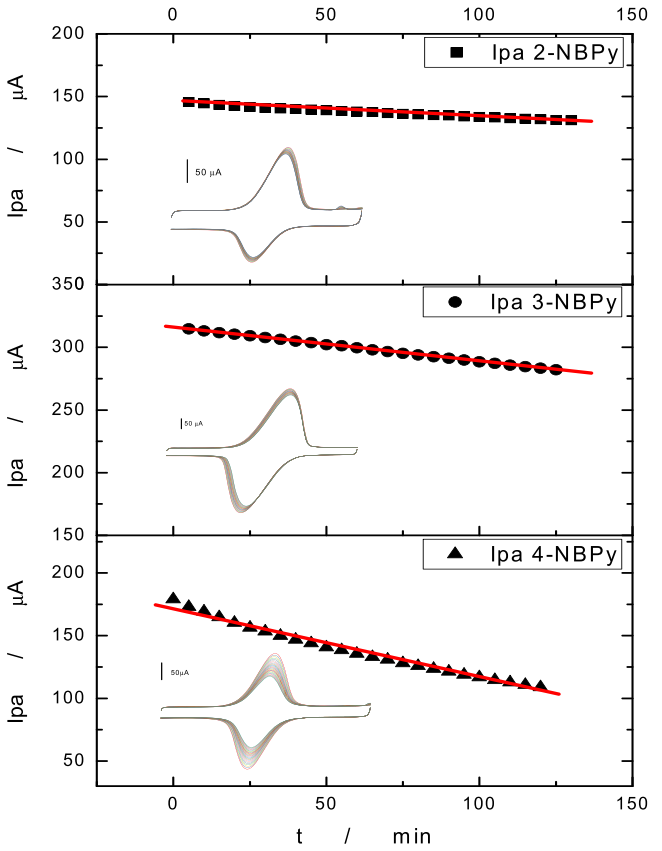

Figure 10. Cyclic voltammogram of the isolated RNHOH/RNO redox pair of 2−, 3−, and 4-NBPy compounds entrapped on GCMWCNTs in 0.1 M Britton-Robinson buffer at pH 7 at 100 mVs^{-1} recorded every 5 min with the same electrode.

The heterogeneous electron transfer rate constant, *ks*, from *Ep* vs log v plots for the NBPy derivatives was calculated. Using x-intercepts for anodic and cathodic branches, as shown in Fig. 8, *va* and *vc* can be estimated to be used in Eq. 5.

$$ks = \frac{\alpha nFvc}{RT} = \frac{(1-\alpha)nFva}{RT} \quad [5]$$

Consequently, using Eq. 5, the calculated heterogeneous electron transfer rate constant *ks* for all of the studied compounds is shown in Table III. All NBPy derivatives showed high *ks* values, which indicates that using them as redox mediators is a possibility. Furthermore, *ks* values calculated from the anodic and cathodic branches are close to each other for every NBPy derivative, and the mean value was reported.

On the other hand, Fig. 8 shows the typical Laviron trumpet-shaped graph, in which the *Epa* and *Epc* at low scan rates are almost independent. This trend indicates a fast charge transfer kinetics in the low scan rates zone. However, as the scan rate increases, the peaks potentials are separate, indicating a limitation in the charge transfer kinetics at fast scan rates. The α and *ks* values obtained indicate a rapid interaction between the NAC and the nanotube network for all compounds regardless of their structural differences.

Furthermore, from the ip_c/ip_a current ratio vs sweep rate in Fig. 9, we can observe a clearly different mechanism for the 2-NBPy derivative compound, wherein the current ratio increased with the sweep rate indicative of charge transfer followed by an irreversible chemical reaction process (EC), as predicted in the seminal work of Nicholson and Shain.[41] This difference is probably because a protonation chemical stage in the 2-NBPy derivative compound is faster than in the other 3- and 4-NBPy derivative compounds, where the chemical stages do not affect the current.

Table IV. Stability study for NBPy derivatives compared with dinitro 3,5-DNBPy.

Compound	Slope (μA/min)	Intercept	r^2	% $Decay_{60}$	% $Decay_{125}$
2-NBPy	−0.116 ± 0.002	145.32 ± 0.19	0.988	6.04	10.59
3-NBPy	−0.288 ± 0.004	314.60 ± 0.27	0.996	5.95	10.12
4-NBPy	−0.559 ± 0.016	171.82 ± 1.09	0.982	24.29	39.20
3,5-DNBPy	−0.239 ± 0.036	182.10 ± 0.02	0.994	9.62	16.88

Stability of entrapped redox mediator hydroxylamine/nitroso derivatives (RNHOH/RNO) from NBPy.—To estimate the stability or persistence of the ArNHOH/ArNO redox pair on the nanostructured platform with NAC, consecutive cyclic voltammograms were performed. As shown in Fig. 10, cyclic voltammetry experiments in the potential window of the RNHOH/RNO redox pair were performed without changing the working electrode in Britton-Robinson buffer at pH 7 at a 100 mVs^{-1} sweep rate. Then, the stability of the redox mediator reaction was estimated by plotting the anodic peak current vs time. The peak current is proportional to the mediator concentration, and a decrease in the peak current indicates desorption of the redox mediator from the nanostructured platform. All compounds possess the same adsorptive tail (butylpyrene), and structural differences are presented in the position of $-NO_2$ related to this adsorptive tail, i.e., *ortho* for 2-NBPy, *meta* for 3-NBPy and *para* for 4-NBPy. For higher slopes, a lower retention is expected. Additionally, for comparative analysis, we incorporated the results obtained in a previous paper[26] using a related dinitro derivative such as 4-(pyrene-1-yl) butyl-3,5-dinitrobenzoate (3,5-DNBPy). Analyzing the slopes shown in Tables IV, 4-NBPy showed the highest slope, and the peak current decreased by 24.29% after 60 min of the experiment and 39.20% after 125 min. For derivatives 2-NBPy and 3-NBPy, excellent stability was observed, and decreases of 6.04% and 5.95%, respectively, were observed after 60 min of the experiment. In conclusion, 2- and 3-NBPy have the highest retention rate in the electrode, even more than 3,5-DNBPy, which has two nitro groups in its structure. For future applications as a redox mediator, the more promising precursors are 2-NBPy and 3-NBPy due to their retention on the nanostructured electrodic platform.

Conclusions

We have synthesized three new 4-(pyren-1-yl)butyl-substituted-nitrobenzoates that include a butylpyrene adsorptive tail to improve π–π interactions with the nanostructured electrode platform. All compounds are susceptible to being trapped at the electrode interface and then reduced to the corresponding hydroxylamine derivatives at peak potentials of 2-NBPy = -0.418 V; 3-NBPy = − 0.461 V; and 4-NBPy = −0.337 V vs Ag/AgCl at pH 7. Consequently, 4-NBPy is the easiest compound to reduce due to the conjugation of the nitro with the carbonyl ester group.

The XRD data confirmed that only 2-NBPy is not planar because the carbonyl ester group is not coplanar with the nitrophenyl group, which would imply loss of the conjugation of the nitro with the carbonyl ester, affecting the electronic properties of the compound.

The withdrawing effect of the ester carbonyl group is not significant in the reduction of the nitro group for the 2-NBPy derivative due to the lack of planarity, as explained above, but once the nitro group is reduced to hydroxylamine, we see that 2-NBPy is the compound with the highest oxidation potential, which would indicate that the nitro group reduction product of 2-NBPy would be planar.

All of the synthesized compounds were electrochemically activated on the nanostructured electrode surface, generating a RNHOH/RNO redox couple, which was electrochemically studied in isolation. From this study, we calculate the heterogeneous electron transfer rate constant for the RNHOH/RNO couple entrapped in the nanostructured electrode, obtaining *ks* values of 2.3, 1.4 and 2 s^{-1} for 2−, 3− and 4-NBPy, respectively.

The present study shows that 2- and 3-NBPy have the highest retention rate in the electrode, even more than 3,5-DNBPy,[26] which has two nitro groups in its structure. For future applications as a redox mediator, the more promising precursors are 2-NBPy and 3-NBPy due to their retention on the nanostructured electrodic platform.

Acknowledgments

We thank FONDECYT (grant no. 1210899) and FONDEQUIP (EQM200266) for their support of this work.

ORCID

C. Barrientos https://orcid.org/0000-0002-1478-2782
R. Moscoso https://orcid.org/0000-0001-5174-7903
J. A. Squella https://orcid.org/0000-0003-0362-4399

References

1. R. Moscoso, E. Inostroza, and J. A. Squella, *Electrochem. Commun.*, **81**61 (2017).
2. G. X. Tham, A. C. Fisher, and R. D. Webster, *Electrochim. Acta*, **357**, 136880 (2020).
3. Y. Zhou, Y. Fang, and R. P. Ramasamy, *Sensors*, **19**, 392 (2019).
4. M. Eguílaz et al., *Current Opinion in Electrochemistry*, **14**, 157 (2019).
5. Y. Si and H. J. Lee, *Current Opinion in Electrochemistry*, **22**, 234 (2020).
6. Z. Liu, V. S. Manikandan, and A. Chen, *Current Opinion in Electrochemistry*, **16**, 127 (2019).
7. M. P. Pujadó, *Carbon Nanotubes as Platforms for Biosensors with Electrochemical and Electronic Transduction.* (Springer, Berlin, Heidelberg) (2014).
8. M. E. David et al., *Nanomaterials*, **11**, 1415 (2021).
9. K. Chen, Y. Li, M. Wang, Y. Wang, K. Cheng, Q. Zhang, J. Kang, and Y. Wang, *Small*, **17**, 2007527 (2021).
10. R. Lei, H. Ni, R. Chen, H. Gu, and B. Zhang, *Electrochem. Commun.*, **93**, 20-24 (2018).
11. T. Saliev, *Journal of Carbon Research*, **5**, 29 (2019).
12. S. Ghosh, A. K. Sood, and N. Kumar, *Science*, **299**, 1042 (2003).
13. C. Lopes, O. Costa, L. da Silva, J. Xavier, A. de Almeida, F. Silva, P. Lima, L. Kubota, and M. Goulart, "Activated nitroaromatics are useful surface redox modifiers in electroanalysis." *Advanced Materials and Systems for Electrochemical Technologies* (Nova Science Publishers, New York, NY) p 73 (2018).
14. H. Park, J. Zhao, and J. P. Lu, *Nano let.*, **6**, 916 (2006) .
15. R. Khan and Y. Nishina, *Nanoscale*, **13**, 36 (2021).
16. M. Cui, S. Ren, S. Qiu, H. Zhao, L. Wang, and Q. Xue, *Surf. Coat. Technol.*, **340**, 74 (2018).
17. M. Kragulj, J. Tričković, B. Dalmacija, Á. Kukovecz, Z. Kónya, J. Molnar, and S. Rončević, *Chem. Eng. J.*, **225**, 144 (2013).
18. A. A. D'Archivio, M. A. Maggi, A. Odoardi, S. Santucci, and M. Passacantando, *Nanotechnology*, **29**, 065701 (2018).
19. R. Moscoso, J. Carbajo, M. Lopez, L. J. Núñez-Vergara, and J. A. Squella, *Electrochem. Commun.*, **13**, 217 (2011).
20. P. Jara-Ulloa, P. Cañete-Rosales, L. J. Núñez-Vergara, and J. A. Squella, *J. Braz. Chem. Soc.*, **22**, 1271 (2011).
21. P. Jara-Ulloa, P. Salgado-Figueroa, C. Yañez, L. J. Nuñez-Vergara, and J. A. Squella, *Electroanalysis*, **24**, 1751 (2012).
22. R. Moscoso, J. Carbajo, and J. A. Squella, *J. Chil. Chem. Soc.*, **59**, 2498 (2014).
23. J. Urzúa, J. Carbajo, C. Yáñez, J. F. Marco, and J. A. Squella, *J. Solid State Electrochem.*, **20**, 1131 (2016).
24. J. Urzúa, C. Yañez, J. Carbajo, and J. A. Squella, *J. Electrochem. Soc.*, **165**, 16 (2018).
25. F. Giroud, K. Sawada, M. Taya, and S. Cosnier, *Biosens. Bioelectron.*, **87**, 957 (2017).
26. R. Moscoso, C. Barrientos, S. Moris, and J. A. Squella, *J. Electroanal. Chem.*, **837** (2019).
27. T. Rębiś, M. Falkowski, G. Milczarek, and T. Goslinski, *ChemElectroChem*, **7**, 2838 (2020).
28. F. J. Ostos, J. A. Lebrón, M. L. Moyá, E. Bernal, A. Flores, C. Lépori, Á. Maestre, F. Sánchez, P. López-Cornejo, and M. López-López, *Int. J. Mol. Sci.*, **22**, 826 (2021).

29. J. A. Squella, S. Bollo, and L. J. Núñez-Vergara, *Curr. Org. Chem.*, **9**, 6 (2005).
30. C. G. Sanz, K. A. Dias, R. P. Bacil, R. A. M. Serafim, L. H. Andrade, E. I. Ferreira, and S. H. P. Serrano, *Electrochim. Acta*, **368**, 137582 (2021).
31. M. Falkowski, T. Rebis, J. Piskorz, L. Popenda, S. Jurga, J. Mielcarek, G. Milczarek, and T. Goslinski, *J. Porphyrins Phthalocyanines*, **21**, 295 (2017).
32. C. Barrientos, P. Barahona, J. L. Guevara, J. A. Squella, and S. Moris, *Z. Kristallogr. NCS*, **234**, 6 (2019).
33. S. Zhang, F. Zhang, Y. Pan, L. Jin, B. Liu, Y. Mao, and J. Huang, *RSC Adv.*, **8**, 5678 (2018).
34. M. C. García-Gutiérrez, A. Nogales, J. J. Hernández, D. R. Rueda, and T. A. Ezquerra, *Opt. Pura Apl.*, **40**, 195 (2007).
35. G. Contreras, C. Barrientos, R. Moscoso, A. Álvarez-Lueje, and J. A. Squella, *Microchem. J.*, **159**, 105422 (2020).
36. J. Urzúa, C. Yañez, J. Carbajo, J. D. Mozo, and J. A. Squella, *Electrochem. Commun.*, **120**, 106852 (2020).
37. J. Kwon, E.-M. Cho, P. Nandhakumar, and S. I. Yang, *Anal. Chem.*, **90**, 13491 (2018) .
38. F. D. Munteanu, N. Mano, A. Kuhn, and L. Gorton, *J. Electroanal. Chem.*, **564**, 167 (2004).
39. M. Santhiago, P. R. Lima, W de J. R. Santos, and A. B de O., L. T. Kubota, *Electrochim. Acta*, **54**, 6609 (2009).
40. E. Laviron, *J. Electroanal. Chem. Interfacial Electrochem.*, **101**, 19 (1979).
41. R. S. Nicholson and I. Shain, *Anal. Chem.*, **36**, 4 (1964).